HHS Public Access

Author manuscript

J Surg Res. Author manuscript; available in PMC 2016 December 01.

Published in final edited form as:

J Surg Res. 2015 December ; 199(2): 296–305. doi:10.1016/j.jss.2015.06.035.

New Continuous-Flow Total Artificial Heart and Vascular Permeability

Jun Feng, MD, PhD[1], **William E. Cohn, MD**[2], **Steven M. Parnis, BS**[2], **Neel R. Sodha, MD**[1], **Richard T. Clements, PhD**[1], **Nicholas Sellke, BS**[1], **O. Howard Frazier, MD**[2], and **Frank W. Sellke, MD**[1]

[1]Division of Cardiothoracic Surgery, Department of Surgery, Cardiovascular Research Center, Rhode Island Hospital, Alpert Medical School of Brown University

[2]Cardiovascular Research Laboratories, Texas Heart Institute at St. Luke's Episcopal Hospital, Houston, Texas

Abstract

Background—We tested the short-term effects of completely non-pulsatile versus pulsatile circulation after ventricular excision and replacement with total implantable pumps in an animal model on peripheral vascular permeability.

Methods—Ten calves underwent cardiac replacement with two HeartMate III continuous-flow rotary pumps. In five calves, the pump speed was rapidly modulated to impart a low-frequency pulse pressure in the physiologic range (10–25 mmHg) at a rate of 40 pulses per minute (PP). The remaining 5 calves were supported with a pulseless systemic circulation and no modulation of pump speed (NP). Skeletal muscle biopsies were obtained before cardiac replacement (baseline) and on postoperative days (POD) 1, 7 and 14. Skeletal muscle tissue water content was measured and morphological alterations of skeletal muscle were assessed. VE-cadherin, phospho-VE-cadherin and CD31 were analyzed by immuno-histochemistry.

Results—There were no significant changes in tissue water content and skeletal muscle morphology within group or between groups at baseline, POD 1, 7 and 14, respectively. There were no significant alterations in the expression/distribution of VE-cadherin, phospho-VE cadherin and CD31 in skeletal muscle vasculature at baseline, POD 1, 7 and 14 within each group or between the two groups, respectively. Although continuous-flow total artificial heart (CFTAH)

Corresponding Author: Frank W. Sellke, M.D., 2 Dudley Street, MOC 360, Division of Cardiothoracic Surgery, Providence, RI 02905, Phone: (401) 444-2732, Fax: (401) 444-2380, fsellke@lifespan.org.

Presented at the 10th Annual Academic Surgical Congress, Feb. 3–5, 2015 Les Vegas, NV

Authors Contribution: Each of the authors listed below have made substantial contributions in each of these three areas: (1) conceiving and designing the study; or collecting the data; or analyzing and interpreting the data; (2) writing the manuscript or providing critical revisions that are important for the intellectual content; and (3) approving the final version of the manuscript. J.F.; W.E.C.; S.M.P.; R.T.C.; N.R.S.; N.S.; O.H.F.; F.W. S:

Disclosure

The authors reported no proprietary or commercial interest in any product mentioned or concept discussed in this article.

with or without a pulse pressure caused slight increase in tissue water content and histological damage scores at POD 7 and 14, it failed to reach statistical significance.

Conclusions—There was no significant adherens-junction protein degradation and phosphorylation in calf skeletal muscle microvasculature after CFTAH implantation, suggesting that short term of CFTAH with or without pulse pressure did not cause peripheral endothelial injury and did not increase the peripheral microvascular permeability.

Keywords

Continuous-flow total artificial heart; Total cardiac replacement device; Tissue edema; Adherens-junction protein; Vascular permeability

1. INTRODUCTION

In recent years, we have witnessed the development and clinical application of several new rotary, or "constant-flow," blood pumps, which are implanted for long-term support of the failing left ventricle.[1–5] Unlike their pulsatile, volume-displacement predecessors, rotary pumps have no flexible membranes, pusher-plates, or prosthetic valves that can wear out, and they are actuated by a single, rapidly spinning impeller.[6–9] The reduced mechanical complexity of rotary pumps dramatically improves their durability and makes them less expensive to produce.[10–13] In addition, these pumps are smaller, quieter, and more energy-efficient than pulsatile pumps. [10–13] Lastly, rotary pumps are inflow-pressure sensitive. They closely imitate the native heart by autonomously increasing pump flow in response to an increasing preload. Therefore, constant-flow technology may be ideally suited for integration into the next generation of permanently implantable cardiac replacement device (CRD).

Clinically, we have observed patients with constant-flow pumps implanted for advanced heart failure who had no clinically detectable pulse. [3, 14] We hypothesized that a CRD of this type will have a different impact on peripheral vascular permeability when operated at a constant speed, or in pulseless mode, compared to when the pump is operated to produce a pulsatile output, and that this difference will be manifest accordingly at the microvascular level. The effects of the absence of pulsatile blood flow on tissue edema and vascular permeability is unknown. Therefore, in this study, we examined the short-term effects of completely non-pulsatile versus pulsatile circulation after ventricular excision and replacement with a newly developed rotary blood pump, HeartMate III (Thoratec Corporation, Pleasanton, CA) in an animal model on peripheral vascular permeability.

2. MATERIALS and METHODS

2.1. Surgical Technique and Monitoring

Ten Corriente-cross calves (body weight: 82.27 ± 4.2 kg, both male and female) were implanted with two HeartMate III constant flow pumps. Each calf received humane care in compliance with the Principles of Laboratory Animal Care (National Society of Medical Research) and the Guide for the Care and Use of Laboratory Animals (National Institutes of

Health Publication no. 85–23, revised 1996). Our Institutional Animal Care and Use Committee approved all the protocols used in this study.[12, 13]

The operative procedure has been described previously, [12, 13] but in summary, each calf was placed in a right lateral recumbency position. The left side of the neck was incised, and the left carotid artery and jugular vein exposed for cannulation for cardiopulmonary bypass (CPB). A concomitant tracheostomy was performed with a size-10 tracheostomy cannula to facilitate respiratory care postoperatively. The chest was entered via a left thoractomy and the left internal thoracic artery was cannulated with a pressure monitor catheter. The power cables and leads of both pumps, along with two ultrasonic flow probes, were tunneled to exit the skin near the left paraspinal aspect of the calf's lumbar area. The pericardium was opened vertically from a point near the phrenic nerve as far as the apex and horizontally near the base of the heart. The heart was then suspended in a pericardial cradle. The calves were systematically heparinized with 3 mg/kg of heparin. Arterial cannulation was performed using appropriately sized cannulas placed in the left carotid artery and descending thoracic aorta. The inferior vena cava and left jugular vein were selectively cannulated with the appropriate (straight or right-angled) venous cannulas, and CPB was initiated. The proximal brachiocephalic artery just above the ascending aortic bifurcation was cross-clamped and transected 1 cm above the aortic and pulmonary valves, respectively. The left and right ventricles were excised by means of transection at the level of the atrio-ventricular groove, and the mitral and tricuspid valves were excised. Teflon-strip supports were used to create a hemostatic connection between the atria and custom-fabricated Dacron/silicone cuffs which were sewn to the right and left artial remnants and attached to the HeartMate III inlets. The outflow grafts of the systemic and pulmonary pumps were measured, divided, and anastomosed end-to-end to the aorta and pulmonary artery, respectively. Both grafts were then deaired, and the pumps were started at low speed while further deairing was performed. The ultrasonic flow probes were placed on each outflow graft. Left atrial, pulmonary artery, and right atrial pressure lines were placed and tunneled out through the chest wall.

Calves were weaned from CPB while systemic and pulmonary pump speeds and flows adjusted to maintain physiologic parameters. After surgical hemostasis was obtained, the CPB cannulas are removed, and purse-string sutures secured. The effects of heparinization were reversed with protamine sulfate. Bilateral chest tubes were placed, and the incisions closed in layers. After vital signs were stable, calves were then transported to the intensive care unit (ICU) for postoperative recovery.

2.2. Pump Control and Operation

Ten calves underwent cardiac replacement with two HeartMate III constant-flow rotary pumps. In the 5 calves, the pump speed were rapidly modulated to impart a low-frequency pulse pressure in the physiologic range (10 – 25 mm Hg) at a rate of 40 pulses/min. The remaining 5 calves were supported with a pulseless circulation and no modulation of pump speed. Motor-drive and levitation-control electronics, which were based on a satellite-printed circuit board arrangement, were incorporated within the lower housing of the HeartMate III. All control parameters were, thus, contained within the pump and can only be changed by means of communication though the external power hub or system controller. A

CRC (cyclic redundancy check), CCITT polynomial was used to ensure that all incoming commands are valid. Each implanted HeartMate III was controlled independently of the other.

For these studies, the HeartMate III pumps were operated at a fixed speed with no variation in pulse pressure or in a pulse mode to vary the pulse pressure. Pulse mode modulated the pump rotor speed between a maximum and minimum level according to 5 key parameters: maximum rotor speed, minimum rotor speed, ramp step (rate of change from minimum to maximum rotor speed), duty cycle (percent of cycle at the maximum pulse speed), and pulse rate (number of cycles/min).

2.3. Postoperative Follow-up and Medical Management

Following surgery, animals were transferred from the operating room table to a stanchion and transported to the ICU for continuous monitoring. Aortic, right atrial, left atrial, and pulmonary artery pressures were monitored for the duration of the study. Indwelling chest tube catheters were attached to an underwater seal suction device and set at an approximately 20-cm H_2O vacuum. Cefazolin (15–30 mg/kg, intravenously [IV]) was given 8 hours after the last intra-operative dose and then given every 8 hours for 2 weeks or at the discretion of the attending/clinical veterinarian or surgeon. Animal were monitored for any signs of discomfort, inflammation, or pain and given butorphanol (0.05–0.4 mg/kg, IV or intramuscularly [IM]) and/or flunixin meglumine (1.1–2.2 mg/kg, IV, IM, or PO), as needed. Water was provided ad lib.

Intravenous heparin was started about 12 hours postoperatively to maintain activated clotting times (ACT) above 200 seconds. Measurements of pulmonary and systemic pump performance, including pump speed in revolutions per minute (rpm), pump power consumption in watts, flow probe data in liters per minute (L/min) and pressure data from the RAP, LAP, PAP, and AoP lines, were recorded continuously throughout the postoperative period by a multichannel data-acquisition system (Ponemah System, version 3.3; Data Sciences International; St. Paul, Minn).

2.4. Tissue Collection

With the aid of local anesthetic and light sedation, skeletal muscle biopsies of the calves' hind limbs were performed in the stanchions under sterile conditions. Baseline specimens were obtained before cardiac replacement and on postoperative days (POD) 1, 7, and 14, respectively. Tissue was immediately frozen in liquid nitrogen for molecular assays or placed in 10% formalin.

2.5. Measurement of Skeletal Muscle Water Content

Skeletal muscle water content was measured by obtaining the wet and dry weights of tissue samples. Skeletal muscle tissue sections were cut, immediately weighed and the wet weight recorded. They were then placed in a 50°C incubator for 48 hours and subsequently weighed again to record the dry weight. The extent of muscle edema was measured by the tissue water percentage, which was calculated by (wet weight-dry weight)/wet weight.

2.6. Histological Assessment

Formalin-fixed and paraffin-embedded tissue sections were cut to 5 μm and stained with hematoxylin and eosin (H& E) to assess the degree of muscle damage. Analysis was carried out on 10 randomly chosen fields in each slide under standard conditions at 20× magnification, and performed by a research technician who was blinded to the treatment given. The histological damage score was performed as follows: disorganization and degeneration of the muscle fibers (0: Normal, 1: Mild, 2: Moderate, 3: Severe); Inflammatory cell infiltration (0: Normal, 1: Mild, 2: Moderate, 3: Severe).[15,16]

2.7. Immunoblotting

The snap-frozen-skeletal muscle-tissue samples (n= 4/group) were dissected and cleaned of fat and connective tissues, then homogenized on ice in a radio-immuno-precipitation assay buffer (RIPA, Boston BioProducts, Ashland, MA) supplemented with protease and phosphatase inhibitors (Roche, Branford, CT). The total lysate protein concentration was measured spectrophotometrically at 562-nm wavelength by using a multi-mode microplate reader (BioTek Instruments, INC, Winooski, VT) with a BCA protein assay kit (Thermo Scientific, Waltham, MA). Total protein was fractionated on 4–20% SDS-PAGE and transferred to a polyvinylidene difluoride membrane (Millipore Corporation, Bedford, MA) with a transfer apparatus (BioRad, Hercules, CA). Membranes were then incubated with 5% nonfat dry milk in 50 mmol/L Tris-HCl, pH 8.0, 100 mmol/L NaCl, and 0.1% Tween 20 (TBST) buffer for 1 hour at room temperature to block nonspecific binding. Membranes were incubated overnight at 4°C with primary rabbit monoclonal or polyclonal antibodies with 1:1000 dilutions against VE-cadherin (Cell Signaling, Danvers, MA). After washing with TBST, membranes were incubated for 1 hour at RT in 2.5% nonfat dry milk in TBST diluted with the appropriated secondary antibody conjugated to horseradish peroxidase. Peroxidase activity was visualized with enhanced chemiluminescence (Thermo Scientific) and the images were captured with a digital camera system (G Box, Syngene, Cambridge, UK). The western blot bands were quantified with densitometry using ImageJ software (National Institute of Health, Bethesda, MD).[17,18]

2.8. Immuno-histochemistry

Skeletal muscle sections were de-paraffinized in xylene, rehydrated in graded ethanol and phosphate-buffered saline solution, and antigen-unmasked with sodium citrate (10 mmol/L, pH = 6.0) followed by phosphate-buffered saline (PBS) wash and blocking with 2%bovine serum albumin in phosphate-buffered saline at room temperature for 2 hours.[17,18] After phosphate-buffered saline wash, overnight incubation with anti- CD3 (Cell Signaling), VE-cadherin (Cell Signaling), and anti-phospho-VE-cadherin (Lifespan Biosciences Inc. Seattle, WA) antibodies (each used 1:50) was performed at 4°C. Anti-mouse, smooth muscle actin (1:1000; Sigma, St Louis, Mo) was used to detect microvascular smooth muscle. Sections were then washed in phosphate-buffered saline and incubated with the appropriate Alexa fluor secondary antibody and mounted using fluorescent mounting medium (Vector Labs, Burlingame, Calif). Tissue labeling with secondary antibody alone or with normal rabbit IgG or serum in place of primary antibody served as a negative control. Tissue was visualized using a Nikon E800 epi-fluorescent microscope system (Nikon Inc. Melville,

NY). Six image photos per slide were taken at same magnificent resolution (20 x Plan Fluor objective) for optical density (intensity) analysis (Spot RT3, Diagnostic Instruments, Sterling Heights MI)

2.9. Statistical Analysis

All data are reported as mean ± S.E.M. Statistical comparisons of the groups were performed by Krukal-Wallis Test (nonparametric test) followed by Dunn's Multiple Comparison Test, Data were analyzed using GraphPad Prism ver. 5.0 (GraphPad Software, San Diego, CA). Probability values of less than 0.05 were considered to be statistically significant.

3. RESULTS

3.1. Hemodynamics

One animal from the pulsatile group died at POD 3 and one animal from the non-pulsatile group died at POD 8. The eight remaining animals (n = 4/group) survived beyond POD 14. The mean arterial pressure (MAP), left (LAP) and right atrial pressure (RAP) were relatively stable during the first 14 postoperative days of the study (Fig. 2A–C). There were no significant differences between pulsatile and non-pulsatile groups in terms of hemodynamic parameters. Both pulmonary and systemic blood flows remained stable (left pump flow: 8.3 ± 0.5 L/min of pulsatile pumps (PP) vs. 8.6 ± 0.6 L/min of non-pulsatile pumps at POD14; right pump flow: 8.4 ± 0.3 L/min vs. 10.4 ± 1.2 L/min (, P>0.05, Fig. 2D, E).

3.2. Tissue Edema

There were no significant changes in skeletal-muscle-tissue water content within group or between the two groups at baseline, POD 1, 7 and 14, respectively (P>0.05, Fig. 3), indicating that there was no evidence of an ongoing increase in tissue edema after POD 14 of CRD.

3.3. Muscle Histology

H&E staining demonstrated skeletal muscle fibers and vessels at corresponding time points in the pulsatile and non-pulsatile groups. Significant skeletal muscle damage was not observed in the two groups at the respective time points (Fig. 4A). The histological damage scores trended to increase after CRD at POD 7 and 14, but failed to reach statistical significance within each group or between the two groups at correspondent time points. (P>0.05, Fig. 4B).

3.4. Adherens-Junction Expression

There were no significant alterations in the expression of endothelial adherens-junction protein VE-cadherin in calf skeletal muscle at baseline, POD 1, 7 and 14 within each group or between the two groups (Fig. 5, P > 0.05, n = 4/group), respectively.

3.5. Endothelial Adherens-Junction Localization

Immunofluorescent staining demonstrated that VE-cadherin, phospho-VE-cadherin and CD 31 (red) co-localized with smooth muscle α-actin (green) to skeletal muscle microvascular endothelial cells (Fig. 6A–C). There were no significant alterations in distribution (intensities) of endothelial adheren-junction proteins VE-cadherin, phospho-VE-cadherin and the endothelial marker CD31 in the calf skeletal muscle microvasculature at baseline, POD 1, 7 and 14 within each group or between the two groups ($P > 0.05$ Fig. 6D, $n = 4$/group), respectively. Phospho-VE-cadherin signaling was not detected in the microvessels of all groups as compared a detectable positive control (Fig. 6B).

4. DISCUSSION

Most patients with bi-ventricular assistant device (BiVAD) support retain some degree of cardiac function and as such, maintain some pulsatility. The change in inflow pressure associated with cardiac systole results in a dramatic increase in instantaneous flow through the LVAD with each heartbeat. Even if the aortic valve is not opening, and no palpable pulse can be detected, the cyclic changes in arterial pressure are brisk and significant. Little is known about steady state completely pulseless flow, which results when the ventricles are excised. In our controlled experimental studies, a sine wave was generated on the arterial pressure waveform by modulating the speed of the pumps in one group, and maintained at constant speed and flow state with a flat arterial pressure wave in the second group.

In these experiments, the pulse rate was intentionally maintained lower than standard physiologic rates due to technical concerns. We experimented with various speed modulation algorithms to determine what impact we could have on the arterial waveform. Due to the inability of the rotor to instantaneously accelerate and decelerate due in part to it's rotational inertia, and due in part to the dampening effect of the blood, we found that at modulation rates greater than 30 per minute, the amplitude of our manufactured pulses, and the rate of change of pressure, were decreased. At 30 modulations per minute, we were able to generate the most natural looking waveform. Perhaps with more sophisticated algorithms, or pumps with lighter rotors, a greater rate may be possible.

We previously explored the physiologic effects of a continuous-flow total artificial heart (CFTAH) in a calf model over a 7 week period.[6, 7] We recently demonstrated that such a device could support normal physiologic parameters for 90 days in a calf.[12, 13] In the current study, we examined the short-term (14 days) effects of completely non-pulsatile versus pulsatile circulation after ventricular excision and replacement with total implantable pumps on peripheral vascular permeability in the calves. We found that non-pulsatile or pulsatile CFTAH did not increase peripheral vascular permeability and tissue edema. Specifically, implantation of CFTAH for 14 days did not cause significant adherens-junction protein phosphorylation/degradation in the calf skeletal muscle microvasculature.

Protein tyrosine phosphorylation plays a critical role in numerous vascular processes including vasomotor regulation and the regulation of vascular permeability mediated through endothelial adherens junctions and other endothelial cell-cell contacts.[19–24] Adherens junctions are cellular contacts that are formed by transmembrane and intracellular

proteins. They are organized in clusters at cell-cell contacts and connect through their cytoplasmic domain with a complex arrangement of transmembrane proteins known as cadherins. Cadherins are single chain transmembrane proteins that interact with other related proteins (β-catenin, plakoglobin, and p120) to promote linkage to the actin cytoskeletal. In vascular endothelium, the major cadherin, VE-cadherin, is bonded to catenins and the actin cytoskeleton.[19–24] They tend to be dynamic and highly regulated by oxygen-derived free radicals, and cytokines such as VEGF. Bacterial lipopolysaccharide (LPS) is known to disrupt endothelial barrier function, in part by protein tyrosine kinase activation, suggesting that systemic organ dysfunction during sepsis may in part be due to an altered state of cell-cell junctions.[24] When adherens junctions are stabilized, VE-cadherin loses tyrosine phosphorylation and binds with plakoglobin and actin, while β-catenin is reduced in the adhesion complex with VE-cadherin.

Experimental and clinical studies have shown that CPB immediately increases vascular permeability and leads to tissue edema. [26–28] We have found that CPB in porcine models and patients leads to immediately increased phosphorylation/degradation of endothelial adherens-junction proteins. [26–28] The present study demonstrates that CFTAH with or without pulse pressure for 2 weeks neither changed the total VE-cadherin expression nor increased phosphorylation/degradation of endothelial adherens-junction proteins. These findings indicate that short term CFTAH with or without pulse pressure maintains endothelial cadherin assembly and integrity of endothelium, suggesting that short term use of CFTAH with or without pulse pressure did not cause peripheral endothelial injury and did not increase the peripheral microvascular permeability, resulting in less tissue edema.

Placement of left and right assist pumps in a compromised heart is challenging due to limited space, and challenges associated with obtaining acceptable lie and drainage of the right pump. In addition, the diseased heart becomes a liability in some cases, as a source of thrombus or by presenting challenging geometry with respect to obtaining unobstructed inflow of the two VADs, especially on the right. In addition, when the heart is left in position, some blood may go through the pumps, and some may be ejected through the native aortic and pulmonary valves. Having multiple blood paths result in areas of flow divergence and areas of flow convergence, each of which can result in areas of low flow or stasis. Perhaps results will be better if the heart is removed, resulting in a single blood path for the systemic and pulmonary circulation.

4.1. Limitations

There are several limitations in the present study. First, the number of animals in each group is relatively small. However, we carefully performed statistical analysis in the relatively small sample size. Eight out of ten animals were included in the current analysis (n = 4/group). Second, although we have recently found that such a device could support a calf for 90 days by maintaining normal physiologic parameters, [6,7,12,13] in the present study we did not report the long term (e.g. 60 days and 90 days) effects of cardiac replacement device with or without pulse pressure on vascular permeability. We will continue to perform additional CFTAH surgical procedures and will obtain enough data for analyzing the long term effects of these devices on maintaining normal hemodynamics and vascular

permeability. Third, because of some of the challenges associated with having two separate controllers and managing balance between the two pumps, we think it is unlikely that this approach will be used with any frequency in the clinical setting. Nevertheless, the small size, dramatically improved durability, and improved power efficiency intrinsic to all rotary blood pumps make their integration into the next generation of TAHs very attractive. Finally, we view this body of work as an effort to learn more about the physiologic effects of decreased or absent pulse as we move closer to the development of an integrated continuous flow total artificial heart.

In conclusion, short term of CFTAH with or without pulse pressure may maintain the integrity of peripheral microvascular endothelium by preventing degradation of endothelial adheren junction proteins and decreasing peripheral microvascular permeability and tissue edema.

Acknowledgments

This research project was supported in part by the National Institute of Health (NIH) R01-HL-090921 (O.H.F), R01 grants-HL-46716 (F.W.S); Rhode Island Foundation-RIF-20123834 and the Institutional Development Award (IDeA) from the National Institute of General Medical Science (NIGMS) of the NIH [5P20-GM103652(Pilot Project) to J.F,]. We also thank Jose PioMagalhae for tissue sample organization.

References

1. Potapov EV, Koster A, Loebe M, Hennig E, Fischer T, Sodian R, et al. The MicroMed DeBakey VAD-Part I: The pump and the blood flow. J Extra Corpor Technol. 2003; 35:274–83. [PubMed: 14979416]
2. Frazier OH, Shah NA, Myers TJ, Robertson KD, Gregoric ID, Delgado R. Use of the Flowmaker (Jarvik 2000) left ventricular assist device for destination therapy and bridging to transplantation. Cardiology. 2004; 101:111–6. [PubMed: 14988632]
3. Frazier OH, Delgado RM III, Kar B, Patel V, Gregoric ID, Myers TJ. First clinical use of the redesigned HeartMate II left ventricular assist system in the United States: a case report. Tex Heart Inst J. 2004; 31:157–9. [PubMed: 15212127]
4. Meyer A, Slaughter M. The total artificial heart. Panminerva Med. 2011; 3:141–154. [PubMed: 21775941]
5. Terracciano CM, Miller LW, Yacoub MH. Contemporary use of ventricular assist devices. Annu Rev Med. 2010; 61:255–70. [PubMed: 20059338]
6. Frazier OH, Tuzun E, Cohn WE, Conger JL, Kadipasaoglu KA. Total heart replacement using dual intracorporeal continuous-flow pumps in a chronic bovine model: A feasibility study. ASAIO J. 2006; 52:145–9. [PubMed: 16557099]
7. Frazier OH, Cohn WE, Tuzun E, Winkler JA, Gregoric ID. Continuous-flow total artificial heart supports long-term survival of a calf. Tex Heart Inst J. 2009; 36:568–74. [PubMed: 20069083]
8. Shiose A, Nowak K, Horvath DJ, Massiello AL, Golding LA, Fukamachi K. Speed modulation of the continuous-flow total artificial heart to simulate a physiologic arterial pressure waveform. ASAIO J. 2010; 56:403–9. [PubMed: 20616704]
9. Khalil HA, Kerr DT, Schusterman MA 2nd, Cohn WE, Frazier OH, Radovancevic B. Induced pulsation of a continuous-flow total artificial heart in a mock circulatory system. J Heart Lung Transplant. 2010; 29:568–73. [PubMed: 20153967]
10. Fumoto H, Horvath DJ, Rao S, Massiello AL, Horai T, Takaseya T, et al. *In vivo* acute performance of the Cleveland Clinic self-regulating, continuous-flow total artificial heart. J Heart Lung Transplant. 2010; 29:21–6. [PubMed: 19782590]

11. Fukamachi K, Horvath DJ, Massiello AL, Fumoto H, Horai T, Rao S, et al. An innovative, sensorless, pulsatile, continuous-flow total artificial heart: Device design and initial *in vitro* study. J Heart Lung Transplant. 2010; 29:13–20. [PubMed: 19782599]
12. Cohn WE, Winkler JA, Parnis S, Costas GG, Beathard S, Conger J, Frazier OH. Eight-year experience with a continuous-flow total artificial heart in calves. ASAIO J. 2014; 60(1):15–8. [PubMed: 24281121]
13. Cohn WE, Winkler JA, Parnis S, Costas GG, Beathard S, Conger J, Frazier OH. Ninety-day survival of a calf implanted with a continuous-flow total artificial heart. ASAIO J. 2014; 60(1):25–30. [PubMed: 24281122]
14. Frazier OH, Myers TJ, Westaby S, Gregoric ID. Clinical experience with an implantable, intracardiac, continuous flow circulatory support device: physiologic implications and their relationship to patient selection. Ann Thorac Surg. 2004; 77:133–42. [PubMed: 14726049]
15. Andrade-Silva AR, Ramalho FS, Ramalho LN, Saavedra-Lopes M, Jordão AA Jr, Vanucchi H, Piccinato CE, Zucoloto S. Effect of NFκB inhibition by CAPE on skeletal muscle ischemia-reperfusion Injury. J Surg Res. 2009; 153:254–262. [PubMed: 18755481]
16. Erkanli K, Kayalar N, Erkanli G, Ercan F, Sener G, Kirali K. Melatonin protects against ischemia/reperfusion injury in skeletal muscle. J Pineal Res. 2005; 39:238. [PubMed: 16150103]
17. Feng J, Liu YH, Chu LM, Singh AK, Dobrilovic N, Fingleton JG, et al. Changes in microvascular reactivity after cardiopulmonary bypass in patients with poorly controlled versus controlled diabetes. Circulation. 2012; 126:S73–S80. [PubMed: 22965996]
18. Feng J, Liu YH, Dobrilovic N, Chu LM, Bianchi C, Singh AK, et al. Altered apoptosis-related signaling after cardioplegic arrest in patients with uncontrolled type 2 diabetes. Circulation. 2013; 128:S144–S151. [PubMed: 24030399]
19. Xiao K, Allison DF, Kottke MD, Summers S, Sorescu GP, Faundez V, et al. Mechanisms of VE-cadherin processing and degradation in microvascular endothelial cells. J Biol Chem. 2003; 278:199–208.
20. Bazzoni G, Dejana E. Endothelial cell-to-cell junctions: molecular organization and role in vascular homeostasis. Physiol Rev. 2004; 84:869–901. [PubMed: 15269339]
21. Yuan Y, Meng FY, Huang Q, Hawker J, Wu HM. Tyrosine phosphorylation of paxillin/pp125FAK and microvascular endothelial barrier function. Am J Physiol. 1998; 275:H84–93. [PubMed: 9688899]
22. Dejana E. Endothelial adherens junctions: implications in the control of vascular permeability and angiogenesis. J Clin Invest. 1996; 98:1949–53. [PubMed: 8903311]
23. Lampugnani MG, Corada M, Caveda L, Breviario F, Ayalon O, Geiger B, et al. The molecular organization of endothelial cell to cell junctions: differential association of plakoglobin, beta-catenin, and alpha-catenin with vascular endothelial cadherin (VE-cadherin). J Cell Biol. 1995; 129:203–17. [PubMed: 7698986]
24. Wong RK, Baldwin AL, Heimark RL. Cadherin-5 redistribution at sites of TNF-alpha and IFN-gamma induced permeability in mesenteric venules. Am J Physiol. 1999; 276:H736–48. [PubMed: 9950877]
25. Bannerman DD, Sathyamoorthy M, Goldblum SE. Bacterial lipopolysaccharide disrupts endothelial monolayer integrity and survival signaling events through caspase cleavage of adherens junction proteins. J Biol Chem. 1998; 273:35371–80. [PubMed: 9857080]
26. Bianchi C, Araujo EG, Sato K, Sellke FW. Biochemical and structural evidence for pig myocardium adherens junction disruption by cardiopulmonary bypass. Circulation. 2001; 104:I319–24. [PubMed: 11568076]
27. Khan TA, Bianchi C, Araujo E, Voisine P, Xu SH, Feng J, et al. Aprotinin preserves coronary cellular junctions and reduces myocardial edema after regional ischemia and cardioplegic arrest. Circulation. 2005; 112(Suppl I):I196–I201. [PubMed: 16159815]
28. Emani S, Ramlawi B, Sodha NR, Li J, Bianchi C, Sellke FW. Increased vascular permeability after cardiopulmonary bypass in patients with diabetes is associated with increased expression of vascular growth factor and hepatocyte growth factor. J Thorac Cardiovasc Surg. 2009; 138:185–91. [PubMed: 19577077]

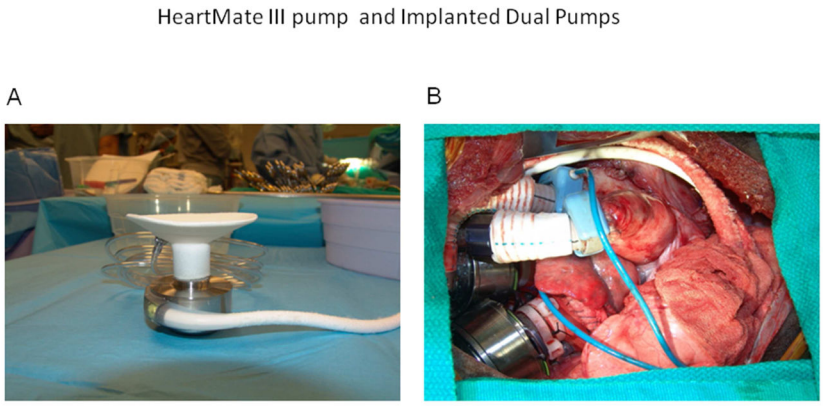

Fig. 1.

A: The HeartMate III pump assembly and driveline. The inflow conduit has a custom silicone-reinforced polyester baffle, and the outflow conduit has a 16-mm polyester graft with an attached 16-mm ultrasonic flow probe (Transonic Systems, Inc., Ithaca, NY). B: Dual HeartMate III pumps implanted in a calf through a median sternotomy incision. The calf's head is to the left.

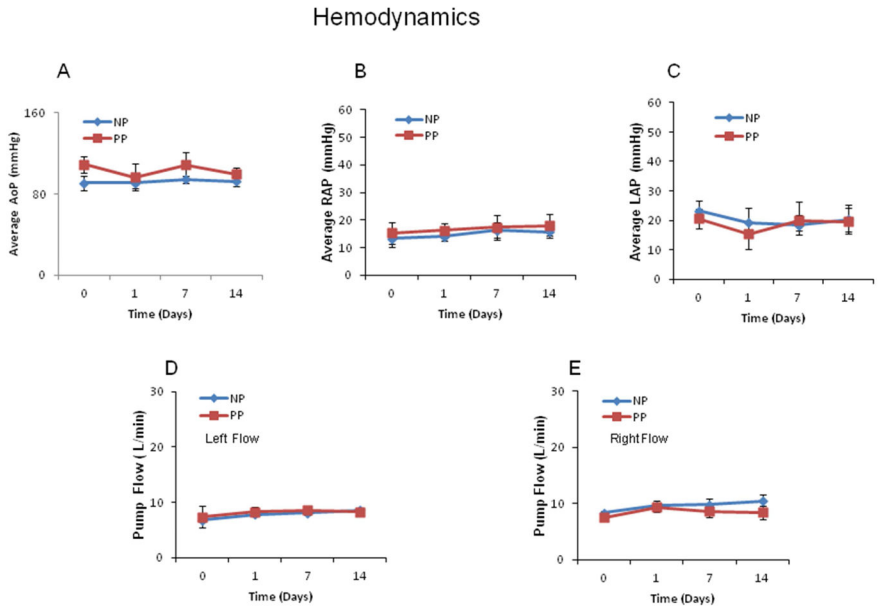

Fig. 2.

During the first 14 days of the study, arterial pressure, left atrial pressure (LAP) and right atrial pressure (RAP) remained relatively steady. The left pump and right pump flow also remained relatively steady. n = 4/group, $P > 0.05$ vs. BS or vs. PP. PP: pulsatile pumps; NP: non-pulsatile pumps.

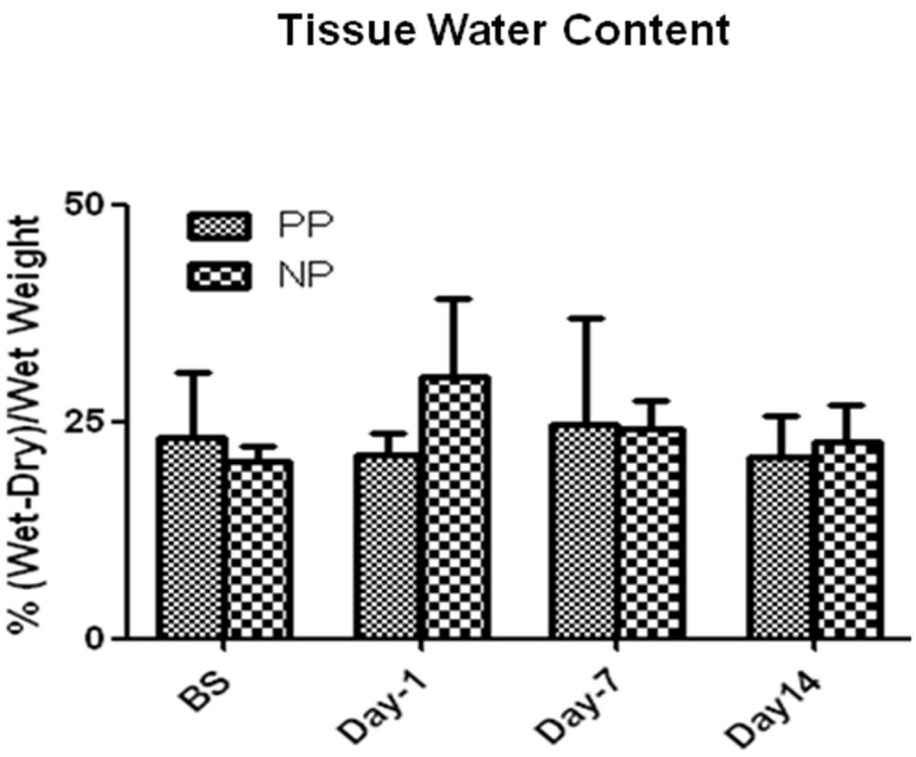

Fig. 3.

Bar graphs represent the skeletal muscle water content from the pulsatile (PP) and non-pulsatile (NP) groups at correspondent time points; n = 4/group, P > 0.05 vs. BS or vs. PP. PP: pulsatile pumps; NP: non-pulsatile pumps.

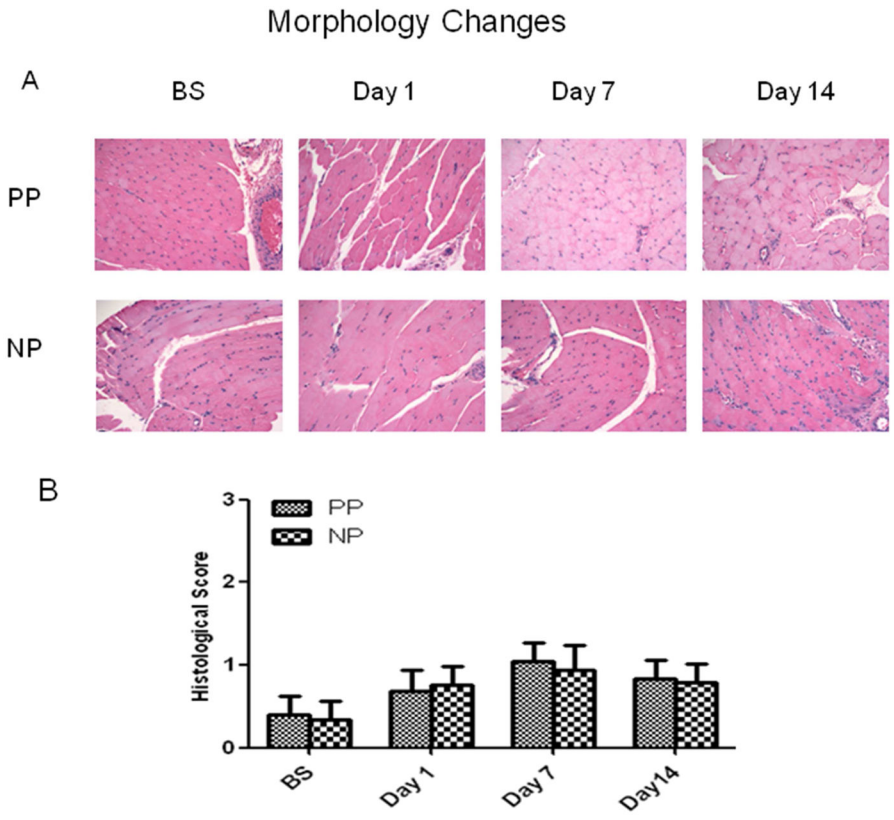

Fig. 4.

A: Representative photomicrographs from the pulsatile and non-pulsatile groups at baseline, postoperative days 1, 7 and 14, respectively. Skeletal muscle sections were processed for hematoxylin-eosin (H&E) staining (magnification: 200). B: Effect of CRD on the skeletal muscle morphological alterations (histological damage score); Scores based on disorganization and degeneration of the muscle fibers, inflammatory infiltration and interstitial edema; n = 4/group $P>0.05$ vs. BS or vs. PP. PP: pulsatile pumps; NP: non-pulsatile pumps.

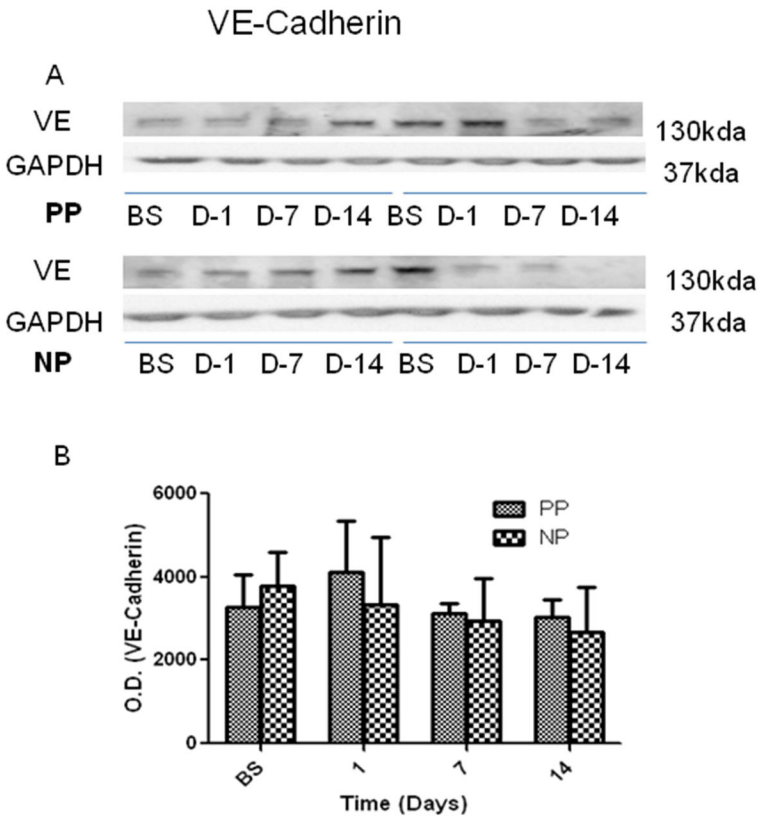

Fig. 5.

(A) Representative immunoblots of calf skeletal muscle for total and phospo-VE-cadherin; (B) Immunoblot quantification shows no significant changes of cadherin protein levels within group or between the two groups. N = 4/group.

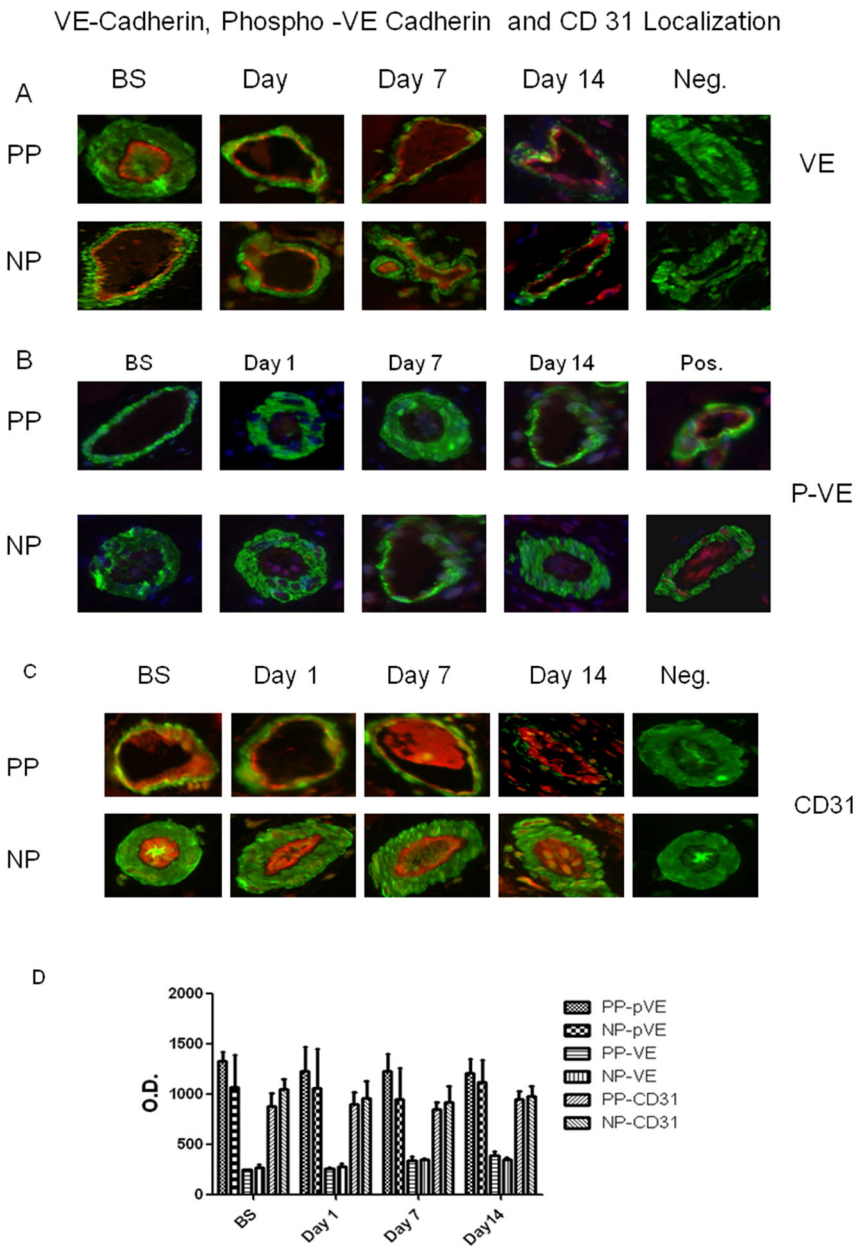

Fig. 6.

Skeletal muscle microvessels were co-stained with VE-cadherin (VE, A), or phospho-VE-cadherin (red) (p-VE, B) and CD31 (C) antibodies or with smooth muscle α-actin antibodies (green). The distribution pattern of VE-cadherin (A), phospho- VE-cadherin (B) and CD 31 along the vascular endothelium in bovine skeletal muscle samples is similar, regardless of sampling time points. D: Densitometric analysis of immunofluorence intensities shows unaltered levels of VE-cadherin, p-VE and CD31 after CRD at respondance time points witn group and between the two groups. n = 4/group P>0.05 vs. BS or vs. PP. PP: pulsatile pumps; NP: non-pulsatile pumps.